Two-dimensional tungsten photonic crystals as selective thermal emitters

Ivan Celanovic,[a] Natalija Jovanovic, and John Kassakian
Laboratory for Electromagnetic and Electronic Systems, Massachusetts Institute of Technology, Cambridge, Massachusetts 02139, USA

(Received 16 April 2008; accepted 21 April 2008; published online 13 May 2008)

This paper presents theory, design, fabrication, and optical characterization of two-dimensional (2D) tungsten (W) photonic crystals (PhC) as selective thermal emitters. We use the photonic band gap of a 2D W PhC, radiating out of a plane of periodicity, to design a selective infrared thermal radiation source that exhibits close to blackbody emittance near the the band gap wavelength and relatively sharp cutoff for wavelengths above the band gap. In addition, we present simple design rules and detailed simulation results for several representative geometries. Microfabrication steps are also presented. Finally, we present detailed experimental results of the optical characterization of three fabricated prototypes that exhibit good agreement with simulation results. © *2008 American Institute of Physics*. [DOI: 10.1063/1.2927484]

The ability of photonic crystals (PhCs) to modify spontaneous emission and as a consequence, their ability to tailor thermal radiation have received significant attention in recent years.[1,2] Indeed, it was shown that PhCs offer unparalleled possibilities for designing thermal radiation sources with properties that are often nonintuitive and significantly deviate from those of typical gray-body sources.

There are two general research areas being pursued with regard to shaping thermal radiation using PhCs. On one hand, PhCs are used to design highly selective narrow-band thermal emitters, exhibiting wavelength, directional and polarization selectivity.[3–6] These structures show promise for applications in infrared (IR) sensors and a variety of IR sources. On the other hand, PhCs are explored to design wide-band thermal emitters exhibiting near-blackbody thermal emission within a given wavelength range and largely attenuated emission outside the given range.[7–9] Applications such as thermophotovoltaic energy conversion, solar-thermophotovoltaic conversion, solar absorbers/reflectors are considered as main drivers behind advances in broadband selective thermal emitters.

In this paper, we focus on a special class of two-dimensional (2D) tungsten (W) PhCs, consisting of a square array of deep cylindrical holes, designed to have close to blackbody emittance in the given broad wavelength range of interest and low emittance outside this range. Several groups reported studies of similar 2D tungsten periodic structures designed to enhance thermal emission. In Ref. 10, the authors reported on a microstructured tungsten emitter that consisted of a square array of posts (with relatively small aspect ratio) fabricated in sputtered tungsten. In Ref. 8, a 2D tungsten grating consisting of periodic array of square cavities, fabricated using electron beam lithography and fast ion beam etching in both single crystal and polycrystalline tungsten, was reported.

In this study we focus on a 2D W PhC that consists of a square array of deep cylindrical cavities with fixed period $a=1$ μm, and different cavity radii and depths. Fabrication of these structures was done using reactive ion etching (RIE) of single crystal tungsten with the etching mask formed using interference lithography (IL). The relatively simple and largely scalable IL process lends itself to large area and batch fabrication proceses.

In the design process we rely on enhancing thermal emission over a relatively broad wavelength range by the mechanism of coupling resonant cavity electromagnetic modes. This enables us to design a wide-bandwidth thermal radiation source with very weak angular and polarization dependence.

The analyzed 2D PhC consists of a periodic array of cylindrical air cavities in tungsten, with radius r, depth d, and periodicity a. For simulating thermal emittance, we used the Ansoft finite element frequency domain electromagnetic solver.[11] We chose the computational cell to have dimension of a by a by $3a$, where a is the period of the PhC in both the $\vec{x}$ and $\vec{y}$ directions, as shown in the inset of Fig. 1. The faces of the computational cell that are perpendicular to the surface

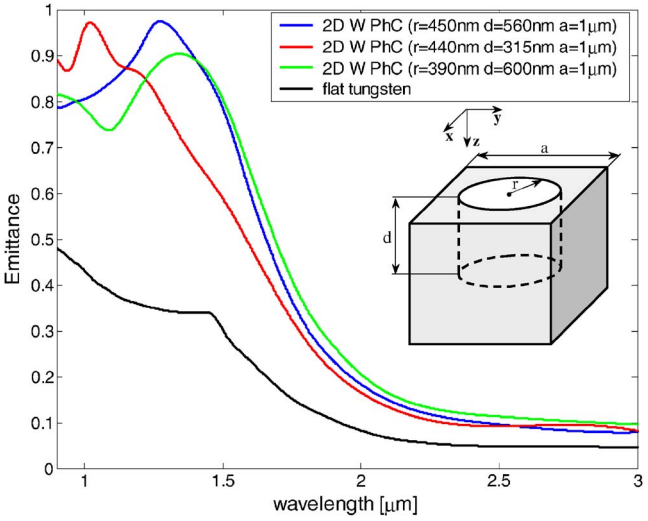

FIG. 1. (Color online) Simulated normal emittance spectra for flat tungsten and three 2D tungsten PhC geometries (using tungsten optical properties from Ref. 12), where incident $\vec{E}$ field is polarized in the $\vec{x}$ direction. 2D tungsten PhCs have following parameters: 2D W PhC I: $r=450$ nm, $d=560$ nm, $a=1$ μm, 2D W PhC II: $r=440$ nm, $d=315$ nm, $a=1$ μm, 2D W PhC III: $r=390$ nm, $d=600$ nm, $a=1$ μm. The inset shows one period of the simulated structure where r is the radius of the holes, d is the hole depth and a is the period of the PhC.

[a]Electronic mail: ivanc@mit.edu.

TABLE I. Estimated and simulated cutoff frequencies for three different 2D W PhC geometries.

	r (nm)	d (nm)	$\lambda_{TE_{111}}$ (nm)	λ_{sim} (nm)
2D W PhC I	450	560	1286	1276
2D W PhC II	440	315	974	1057
2D W PhC III	390	600	1184	1345

of the PhC are chosen to have periodic boundary conditions, while faces parallel to the surface are defined as perfectly matched layers. We illuminate the PhC with a normally incident plane wave (with electric field polarized in the $\vec{x}$ direction) and calculate the spectral reflectance $R(\lambda)$ of the PhC which is related to the emittance $E(\lambda)$ through Kirchhoff's law as $E(\lambda)=1-R(\lambda)$ [since the PhC is opaque and thus transmittance $T(\lambda)=0$].

Simulation results for normal emittance of flat tungsten and three different 2D tungsten PhC geometries are given in Fig. 1. For simulation purposes we used tungsten optical properties that are given in Ref. 12. All simulated PhC's exhibit large emittance enhancement for wavelengths shorter than 2 μm, compared to flat tungsten. In addition, resonantly enhanced emittance peaks, which are directly related to the cylindrical cavity cutoff mode, are evident in all cases.

The signature resonant emission peaks, shown in Fig. 1, correspond to the lowest order transverse electric (TE) resonant mode of the cylindrical cavity. The TE mode frequencies of the finite depth cylindrical cavity with one base of the cylinder exposed to free space can be approximated as

$$\omega_n = \sqrt{\left(\frac{l}{4}\frac{r}{d}\right)^2 + \left(\frac{\xi'_{mn}}{2\pi}\right)^2}, \tag{1}$$

where, ξ'_{mn} is the nth root of the mth order Bessel function derivative, d and r are the depth of the cylinder and the cylinder radius, respectively (as defined in Fig. 1), and l is an integer number.[13] Cavity mode frequencies are expressed in normalized frequency units of $2\pi c/r$. A similar equation can be used to estimate the TM mode resonance if ξ'_{mn} is replaced with ξ_{mn}, where ξ_{mn} is the nth root of the mth order Bessel function. The approximation made in Eq. (1) is that the semiopen cavity can be modeled as a completely enclosed metallic cylinder cavity of depth $2d$. The comparison of the cutoff frequencies obtained from simulation and with the approximate analytical expression (1), is given in Table I for three different PhC geometries. The estimated and simulated resonant mode frequencies, as seen from Table I, are within 10% margin of error.

Tailoring the cutoff mode frequency through geometrical modification of the PhC parameters, gives us the freedom to design a selective thermal emitter with a precisely positioned spectral cutoff, thus matching our particular design specifications. In addition, due to the resonant nature of the emittance enhancement, all three prototypes exhibit very sharp cutoff.

Apart from high emittance below the cutoff wavelength and sharp cutoff, low emittance at long wavelengths is of paramount importance for many applications. Although, there is no closed form analytical expression for the PhC effective dielectric constant that could guide us in the design process, one could use for example the analytic constraint for

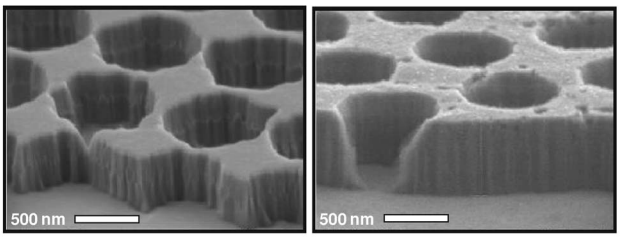

FIG. 2. SEM images of two fabricated 2D single crystal tungsten PhC samples with following parameters: (a) 2D W PhC I: $r=450$ nm, $d=560$ nm, $a=1$ μm and (b) 2D W PhC III: $r=390$ nm, $d=600$ nm, $a=1$ μm.

the effective dielectric constant provided by Weiner bounds, as in Ref. 14. Specifically, for a two-material composite the effective dielectric constant is bounded by

$$(f_1\varepsilon_1^{-1} + f_2\varepsilon_2^{-1})^{-1} \leqslant \varepsilon_{\text{eff}} \leqslant (f_1\varepsilon_1 + f_2\varepsilon_2), \tag{2}$$

where f_1 and f_2 are the volume fractions of the materials with dielectric functions ε_1 and ε_2, and ε_{eff} is the effective dielectric constant. The upper bound of the dielectric constant gives us a good estimate for the lower bound on the 2D W PhC emittance for long wavelengths. For example, for the PhC with $r=440$ nm, $d=315$ and $a=1$ μm, we obtain volume fractions of $f_1=0.6$ and $f_2=0.4$ which gives us the emittance $E(\lambda=3\ \mu\text{m})=0.074$. The error in this case is less than 3% compared to simulation results of the same structure. The importance of the lower bound on the long-wavelength emittance is that it establishes an important design tradeoff between above and below band gap emittance. To minimize above band gap emittance requires minimization of the cavity radius, while reducing the cavity radius, reduces the emittance above the band gap due to weaker outcoupling of the cavity modes.

The scanning electron microscope (SEM) images of three fabricated PhC samples are shown in Fig. 2. The detailed explanation of the microfabrication steps is given in Ref. 15, but for the sake of completeness we present a short overview here.

The fabrication process consists of two major parts: lithography and etching. The sample pattern was produced using laser IL, a simple yet powerful approach that enables fast, large-scale fabrication of a variety of micro- and nanoscale patterns. The pattern is then transferred into the underlying tungsten substrate by etching. The fabrication process steps are illustrated in Fig. 3.

The chromium (Cr) "hard-mask" layer is deposited using electron-beam evaporation. The two lithography layers—antireflective coating (ARC) and photoresist (PR)—are applied using a spinning stage. The spinning rate is used to achieve optimal thicknesses for the ARC and PR, which were calculated to minimize surface reflectance. The PR layer captures the lithographic pattern, while the ARC has a feature-enhancing role. The principle behind the laser IL technique is that of the interference of two coherent light beams. Using a laser source and a mirror, a variety of interference patterns is created by changing the angle between the mirror and the sample. The mirror angle determines the period of the structure, while the duration of exposure determines the cavity radius. After lithography, the pattern is developed using a commercial PR developer.

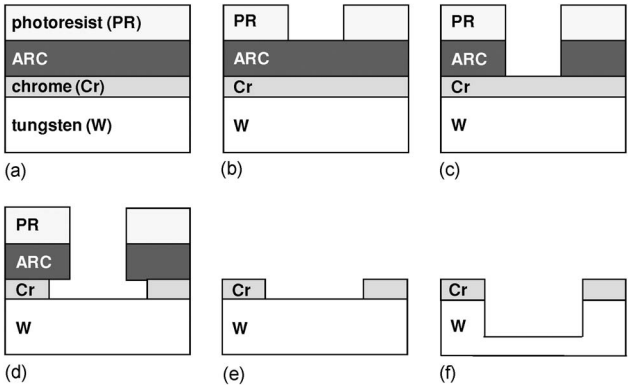

FIG. 3. Flowchart of the 2D W PhC microfabrication process.

Oxygen-based RIE is used to transfer the pattern from the PR into the ARC layer. RIE is a highly directional low-pressure dry gas plasma etching technique. The chromium wet etch process transfers the pattern from the ARC layer into the chromium hard-mask layer. Having served its purpose, the remaining ARC was removed using the same RIE oxygen-based recipe.

The final etch step is a carbon-tetrafluoride-based tungsten RIE. The depth to which tungsten can be etched is limited by the thickness of the chromium mask. In our particular case, 50 nm of chromium lasted until a depth of approximately 600 nm is etched in the tungsten.

We used a spectral reflectance measurement as the central tool in establishing the optical properties of fabricated 2D W PhC samples. Spectral emittance at room temperature is therefore expressed as $E(\lambda)=1-R(\lambda)$. The measurement results are shown in Fig. 4. We show measurements for PhCs and flat tungsten depicted with solid lines while dashed lines show the simulation results as previously discussed. All, three samples exhibit sharp cutoff and near unity emittance at the resonant wavelength. However, the emittance of all the samples above 1.7 μm is larger than the simulated emittance due to larger emittance of the flat tungsten substrates compared with the reference values (which were obtained using optical properties of tungsten from Ref. 12) in that region, and due to nonperfect shape and uniformity of the cavities, as seen in Fig. 2. Fabricated PhC nonuniformity is stemming from nonideal cylindrical cavities and their nonuniform size. On the other hand, we can see a very good agreement between the resonant wavelength peaks in the measurements and simulations. Nevertheless, large emittance enhancements above the cutoff have been demonstrated and highly wavelength-selective emission has been confirmed.

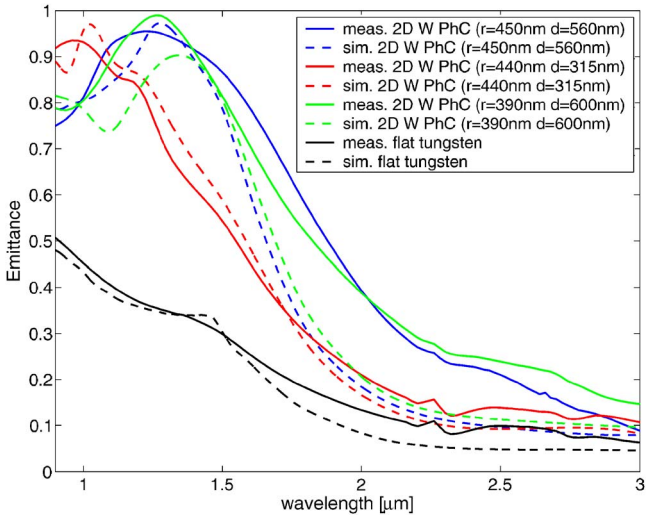

FIG. 4. (Color online) Measured and simulated normal emittance for flat tungsten and three 2D W PhC.

In conclusion, we have shown that a 2D tungsten PhC is a good candidate for the design of a class of broadband highly selective thermal radiation sources. We have demonstrated a straightforward and largely scalable microfabrication process that allows for exceptional control over PhC fabrication parameters.

The ability to adjust the cutoff wavelength, by changing the geometrical parameters of the structure, enables us to tailor the radiation properties for the desired application. For example, for thermophotovoltaic applications, these would allow us to use a 2D W PhC as selective emitter that can be tailored and optimized for different photovoltaic diode materials with different electronic bandgaps, such as GaSb, InGaAs, and InGaAsSb. Furthermore, this approach paves the way toward a variety of selective thermal radiation sources for IR applications that can easily be fabricated using standard and largely scalable microfabrication techniques. Our fabrication process is clearly not restricted to tungsten; materials such as platinum, silver, molybdenum, etc., could easily be used, thus allowing for additional degrees of freedom in tuning the emission properties.

This research was supported in part by the Toyota Motor Corporation, The Sheila and Emmanuel Landsman Foundation and the U.S. Army Research Office through the Institute for Soldier Nanotechnologies.

[1]E. Yablonovitch, Phys. Rev. Lett. **58**, 2059 (1987).
[2]S. John, Phys. Rev. Lett. **58**, 2486 (1987).
[3]J. J. Greffet, R. Carminati, K. Joulain, J. P. Mulet, S. Mainguy, and Y. Chen, Nature (London) **416**, 61 (2002).
[4]M. U. Pralle, N. Moelders, M. P. McNeal, I. Puscasu, A. C. Greenwald, J. T. Daly, E. A. Johnson, T. George, D. S. Choi, I. El-Kady, and R. Biswas, Appl. Phys. Lett. **81**, 4685 (2002).
[5]I. Celanovic, D. Perreault, and J. Kassakian, Phys. Rev. B **72**, 075127 (2005).
[6]D. L. C. Chan, I. Celanovic, J. D. Joannopoulos, and M. Soljačić, Phys. Rev. A **74**, 064901 (2006).
[7]C. M. Cornelius and J. P. Dowling, Phys. Rev. A **59**, 4736 (1999).
[8]H. Sai, Y. Kanamori, and H. Yugami, Appl. Phys. Lett. **82**, 1685 (2003).
[9]J. G. Fleming, S. Y. Lin, I. El-Kady, R. Biswas, and K. M. Ho, Nature (London) **417**, 52 (2002).
[10]A. Heinzel, V. Boerner, A. Gombert, B. Blasi, V. Wittwer, and J. Luther, J. Mod. Opt. **47**, 2399 (2000).
[11]*Ansoft High Frequency Structure Simulator Manual* (Ansoft Corporation, Pittsburgh, PA, USA, 2001).
[12]E. D. Palik, *Handbook of Optical Constants of Solids* (Academic, Orlando, 1985).
[13]J. Roumeliotis, J. Electromagn. Waves Appl. **11**, 185 (1997).
[14]D. E. Aspnes, Am. J. Phys. **50**, 704 (1981).
[15]N. Jovanović, I. Čelanović, and J. Kassakian, *American Institute of Physics Conference Series* (American Institute of Physics, Melville, NY, 2007), Vol. 890, pp. 47–55.